A PRESSURE TRAVERSE ALGORITHM FOR MULTILATERAL OIL AND GAS WELLS

Bruno Ramon Batista Fernandes

brbfernandes@utexas.edu

Center for Petroleum and Geosystems Engineering, The University of Texas at Austin

200 E. Dean Keeton St., Stop C0300, Austin 78712, Texas, USA

Francisco Marcondes

marcondes@ufc.br

Department of Metallurgical Engineering and Materials Science, Federal University of Ceará

Campus do Pici, Bloco 729, 60440-554, Ceará, Fortaleza, Brazil

Kamy Sepehrnoori

kamys@mail.utexas.edu

Center for Petroleum and Geosystems Engineering, The University of Texas at Austin

200 E. Dean Keeton St., Stop C0300, Austin 78712, Texas, USA

Abstract. *Pressure traverse algorithms are important to determine the pressure distribution and rates along oil and gas wells, allowing the coupling of surface and subsurface parameters. These algorithms assume the well is divided into several segments and are usually derived assuming no fluid accumulation along well. The fluid flow patterns (bubble, slug, transition, and mist) are incorporated into the calculations of the pressure drop due to friction and fluid slippage. While many pressure traverse algorithms are available in the literature, just a few are devoted for multilateral wells. In this paper, a recursive pressure traverse algorithm for multilateral wells is presented. We assume that the well can have vertical, curved, and or horizontal sections. The pressure drop in horizontal section is neglected. Two phase flow (oil and gas) is considered with four flow patterns: bubble, slug, transition, and mist flow. The fluid properties are modeled as Black-Oil and the wellbore is coupled to a basic reservoir through a productivity index and each lateral is assumed to penetrate different producing formation layers. The results are presented in terms of pressure distribution, production rates for several well head pressures, etc. The algorithm was able to converge for an arbitrary number of laterals keeping property continuity along the wellbore.*

Keywords: *Pressure traverse, Multilateral wells, Multiphase flow.*

1 INTRODUCTION

Pressure traverse calculations are used to obtain the pressure profile along oil and gas wells as well as other important parameters such as gas-oil ratio, and production rates in the well segments. Such computations are important to determine the well deliverability, which combined with the inflow performance can provide the production rates, given a well head pressure, and vice and versa. Algorithms for pressure traverse are also important tools for coupling the surface and subsurface controlling parameters of a well.

The complexity of obtaining such well profiles in oil wells increase due to the multiphase flow that is established. Such complexity comes from the different flow patterns that can be stablished at different conditions, which produces extremely different friction losses along the tubing. There are two kinds of methods for the description of multiphase flow on production strings: experimental correlations and mechanistic models. The models based on experimental correlations have bigger limitations, but result in simpler and quicker algorithms, while those based on mechanistic models are more reliable, but also more expensive.

Several experimental based approaches for multiphase flow are available in the literature, and are a combination of several different sets of correlations for individual flow patterns. Orkiszewski (1967) presented a theory for multiphase flow in vertical pipes considering four flow patterns: bubble, slug, transition, and mist flow. Taitel and Dukler (1976) proposed a theoretical map for predicting the flow regime in vertical pipes. Another popular approach for computing the pressure gradient in vertical pipes is the modified Hagedorn and Brown method (Brown, 1977), which is based on the work of Hagedorn and Brown (1965). Beggs and Brill (1973) developed an empirical approach for flow regimes in horizontal pipes and extended these for pipes with any inclination. However, the flow regime obtained when using this model are those of a perfectly horizontal pipe and are not adequate for vertical pipes (Economides et al., 1994). Mechanistic models are based on conservation laws and were introduced by Taitel and Dukler (1976) and Taitel et al. (1980) for two phase flow. Recently, Shirdel and Sepehrnoori (2012) presented a compositional transient two-phase mechanistic approach.

Despite of the general pressure gradient laws presented by the authors, algorithms for calculating pressure profile in multilateral wells are rather scarce. On face of such fact, an algorithm for back-calculating the pressure distribution in wells with an arbitrary number of laterals and connections is presented. Herein, each lateral is assumed to be fully drilled into a producing formation, and its contribution to the production string is obtained through inflow performance relationships (IPR). The lateral is connected to the tubing through a curved segment. The Orkiszewski theory is used for the vertical sections of the tubing. Friction losses are negligible for the curved segments and the Beggs and Brill (1973) pressure gradient equation is used. We assume that each lateral is drilled through isolated formations, which are modeled using a “tank model”, a model that discretizes the reservoir as a single control-volume and also known as zero dimension. The tank model is useful for primary production, and allow the production forecasting. A well with two laterals is illustrated in Figure 1, for better understanding of the problem.

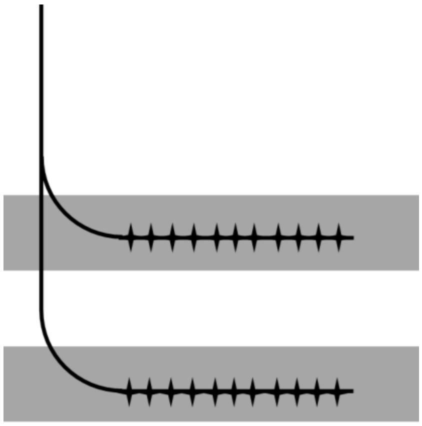

Figure 1. Two Lateral well.

2 PHYSICAL MODEL

In this section, the correlations and models used for calculate important fluid properties are presented. Later, the models used to estimate pressure drop for multiphase and single phase will be presented.

2.1 Fluid Properties

Several oil and gas properties are important in the oil and gas production system. For the models considered here, properties such as gas solution ratio, densities, viscosities, interfacial tension, formation volume factor, bubble pressure, and volumetric rates are considered. The black-oil model is used for describing the fluid. The equations presented in this subsection have been properly converted from Field units to SI units.

The solution gas-oil ratio is estimated for pressures below the bubble point following Vazquez and Beggs (1980) equations as

$$R_s = \begin{cases} \dfrac{0.178\gamma_g \left(\dfrac{P}{6894.76}\right)^{1.0937}}{27.64} 10^{\frac{11.172\gamma_o}{1.8T+0.33}} & for \quad \gamma_o \le 30^o\, API \\ \dfrac{0.178\gamma_g \left(\dfrac{P}{6894.76}\right)^{1.187}}{56.06} 10^{\frac{10.393\gamma_o}{1.8T+0.33}} & for \quad \gamma_o > 30^o\, API \end{cases} . \tag{1}$$

where R_s is the solution gas-oil ratio in m^3/m^3, γ_g is the gas specific gravity, T is the temperature in K, γ_g is the oil gravity in API, and P is the pressure in Pa.

For pressure above the bubble point the solution gas-oil ratio is constant and can be obtained by replacing P in Eq. (1) by the bubble pressure P_b.

The oil formation volume factor for pressures below the bubble point is calculated as (Vazquez and Beggs, 1980)

Proceedings of the XXXVIII Iberian Latin-American Congress on Computational Methods in Engineering
P.O. Faria, R.H. Lopez, L.F.F. Miguel, W.J.S. Gomes, M. Noronha (Editores), ABMEC, Florianópolis, SC, Brazil, November 5-8, 2017.

$$B_o = \begin{cases} 1 + 2.623\times10^{-3} R_s + 0.1751\times10^{-4} F - 1.01575\times10^{-7} R_s F \quad for \quad \gamma_o \le 30^o API \\ 1 + 2.620\times10^{-3} R_s + 0.11\times10^{-4} F + 0.75006\times10^{-8} R_s F \quad for \quad \gamma_o > 30^o API \end{cases}, \tag{2}$$

where

$$F = \left(1.8T - 519.67\right)\frac{\gamma_o}{\gamma_g}. \tag{3}$$

For pressures above the bubble point, the oil formation factor is calculated as (Vazquez and Beggs, 1980)

$$B_o = B_{ob} \exp\left(c_0 \left(P_b - P\right)\right), \tag{4}$$

where

$$c_0 = \frac{-1.433 + 28.05 R_s + 17.2(1.8T - 459.67) - 1.180\gamma_g + 12.61\gamma_o}{\dfrac{P}{6894.76}\times10^5}. \tag{5}$$

In Eq. (4), the oil formation volume factor at the bubble pressure (B_{ob}) is computed by setting the R_s obtained at P_b into Eq. (2).

The oil density is calculated as (Economides et al., 1994)

$$\rho_o = 16.0185 \frac{\left[8830/\left(131.5+\gamma_o\right)\right] + 0.0763521\gamma_{gd} R_s}{B_o}, \tag{6}$$

where the γ_{gd} is the dissolved gas specific gravity.

2.2 Fluid flow model

For computing the rate and pressure profile along the well under a given well head pressure, an inflow performance relation (IPR) and a well deliverability curve are required. Several IPR are available in the literature to provide a relationship between the drawdown pressure and the production rate. These models predict the production rate of a reservoir into the well, but do not provide enough information if that well can actually produce without artificial lift techniques. Well deliverability models are based on the conservation of mechanical energy. The models and hypothesis used in this work are presented next.

The presented numerical simulator only considers the cases at which oil phase flows alone, and oil and gas phases flow simultaneously. For the case of single phase (oil flow), we consider the mechanical energy equation for incompressible flow. This was considered a reasonable approach as the only thing that will change density, in this case, is the temperature, which has quite small change for the size of the segments considered in this type of simulation. The pressure drop for single phase system is computed as

$$-\frac{P_0 - P_L}{\Delta L} = \frac{\Delta P}{\Delta L} = \bar{\rho}_o \frac{u_L^2 - u_0^2}{2\Delta L} + \bar{\rho}_o g \sin\alpha + \frac{2\bar{\rho}_o \bar{f}_f \bar{u}^2}{D}, \tag{7}$$

where ΔL is the length of a given segment, $\bar{f}_f$ is the fanning friction factor evaluated at the average velocity, $\bar{\rho}_o$ is the average oil density in the segment, $\bar{u}_o$ is the oil average velocity, and D is the tubing diameter.

The pressure at a lower depth is then calculated as

$$P_0 = P_L - \Delta P \,. \tag{8}$$

For laminar flow, Reynolds number smaller than *2300*, the fanning factor is calculated from the analytical equation as (Bird et al., 2007)

$$f = \frac{16}{\mathrm{Re}} , \tag{9}$$

where the Reynolds number, in this case, is computed as

$$\mathrm{Re} = \frac{\bar{\rho}_o \bar{u}_o D}{\bar{\mu}_o} . \tag{10}$$

The turbulent flow here was assumed to start at Reynolds number greater than *2300*, which means we assume the transition zone as a fully turbulent. For this flow regime, the Colebrook-White equation (Colebrook and White, 1937) is used to calculate the fanning friction factor.

$$\frac{1}{\sqrt{f_f}} = -4\log_{10}\left(\frac{\varepsilon}{3.7065D} + \frac{1.2613}{\mathrm{Re}\sqrt{f_f}} \right), \tag{11}$$

where ε is the tube roughness.

Equation (11) is solved iteratively using the Newton's method. The friction factor obtained through Chen equation (Chen, 1979) is used as initial guess for the iterative procedure, and is given below:

$$\frac{1}{\sqrt{f_f}} = -4\log_{10}\left(\frac{\varepsilon}{3.7065D} - \frac{5.0452}{\mathrm{Re}} \log\left(\frac{1}{2.8257}\left(\frac{\varepsilon}{D}\right)^{1.1098} + \frac{5.8506}{\mathrm{Re}^{0.8981}} \right)\right). \tag{12}$$

Multiphase flow is considered when the pressure is below the bubble pressure. At this point, free gas is present and a two phase flow takes place. For vertical sections of the well, the Orkiszewski (1967) theory is used. Orkiszewski theory considers several other theories and improvements, and assume the pressure drop along a vertical well segment as

$$\frac{\Delta P}{\Delta L} = \frac{\bar{\rho}_k g + \dfrac{\Delta P_f}{\Delta L}}{1 - C_1} , \tag{13}$$

where $\Delta P_f / \Delta L$ is the pressure drop due to friction, and C_1 is part of the kinetic energy term after being approximated by Boyle's law. The kinetic energy term is given as

$$X = C_1 \Delta P , \tag{14}$$

with

Proceedings of the XXXVIII Iberian Latin-American Congress on Computational Methods in Engineering
P.O. Faria, R.H. Lopez, L.F.F. Miguel, W.J.S. Gomes, M. Noronha (Editores), ABMEC, Florianópolis, SC, Brazil, November 5-8, 2017.

$$C_1 = \frac{\bar{\rho}_k \bar{u}_m \bar{u}_g}{\bar{P}}, \tag{15}$$

where $\bar{u}_m$ is the mass averaged velocity, $\bar{u}_g$ is the gas velocity, and $\bar{\rho}_k$ is the mixture average mass density. The mass averaged velocity is calculated as

$$u_m = \frac{q_{ostd}\left(\rho_o + \rho_g R_s\right)_{std}}{\rho_k A}. \tag{16}$$

where q_{ostd} is the oil rate at standard conditions.

The use of approximated velocities to u_m were leading to C_1 greater than *1*. Therefore, using this makes the formulation more stable.

The liquid hold up, gas slippage velocity, and pressure drop due to friction will be a function of the flow pattern. We considered all flow regimes: slug, mist, build, and transition. Further details can be found in Orkiszewski (1967).

2.3 Inflow Performance Ratio

The Bendakhlia and Aziz (1989) Inflow Performance Relation (IPR) has been used in the simulator presented in this work. This IPR model was proposed for reservoir pressures below the bubble point as

$$q_o = q_{o,\max}\left[1 - V\frac{P_{wf}}{P_{res}} - (1-V)\left(\frac{P_{wf}}{P_{res}}\right)^2\right]^n, \tag{17}$$

where, for pseudo-steady state,

$$q_{o,\max} = \left(\frac{1}{1.8}\right)\frac{1.4596\times10^{-9} k k_{ro} h P_{res}}{B_o \mu_o \left[\ln\left(0.472 r_e / r_w\right) + s\right]}. \tag{18}$$

where P_{wf} is the bottom hole pressure, h is the reservoir thickness, k_{ro} is the oil relative permeability, μ_o is the oil viscosity, k is the reservoir permeability, P_{res} is the reservoir average pressure, s is the skin factor, r_e is the equivalent radius, r_w is the well radius, and V and n are parameters.

For obtaining a version of Eq. (17) that works well for reservoir pressures over the bubble point, the superposition principle was applied, in a similar process to that used to generalize the Vogel IPR, which yields

$$q_o = \begin{cases} q_b + q_v\left[1 - V\dfrac{P_{wf}}{P_b} - (1-V)\left(\dfrac{P_{wf}}{P_b}\right)^2\right]^n, & for \quad P_{wf} \le P_b \\ q_b, & for \quad P_{wf} > P_b \end{cases}, \tag{19}$$

where

Proceedings of the XXXVIII Iberian Latin-American Congress on Computational Methods in Engineering
P.O. Faria, R.H. Lopez, L.F.F. Miguel, W.J.S. Gomes, M. Noronha (Editores), ABMEC, Florianópolis, SC, Brazil, November 5-8, 2017.

$$q_b = \frac{1.4596\times10^{-9} k k_{ro} h\left(P_{res}-P_b\right)}{B_o\mu_o\left[\ln\left(0.472 r_e / r_w\right)+s\right]}, \tag{20}$$

and

$$q_v = \left(\frac{1}{1.8}\right)\frac{q_b P_b}{P_{res}-P_b}. \tag{21}$$

The values of v and n were obtaining through an integral averaging of the data produced by Bendakhlia and Aziz (1989). The values obtained were: $V=0.191334$ and $n=1.067955$.

The effect of the length for the horizontal lateral is included into a pseudo-skin factor (s_{well}). In order to calculate such skin, the well is assumed to have infinite conductivity, and it can be approximated as a fracture. The effective well radius can be computed for infinite conductivity fracture from the data given by Nguyen (2016), which provides that, for infinite conductivity fractures the quotient of the effective radius to the fracture length is constant and equals to *0.5*.

The fracture length is related to the well length as

$$x_f = 0.5L. \tag{22}$$

Therefore, the effective radius will be

$$r_w^{'} = L/4. \tag{23}$$

The skin factor can be computed from the following equation (Economides et al., 1994)

$$r_w^{'} = r_w e^{-s_{well}}, \tag{24}$$

or

$$s_{well} = \ln\left(\frac{r_w}{r_w^{'}}\right). \tag{25}$$

The pseudo-skin is used into Eqs. (17) to (21) to include the effect of the horizontal well length.

2.4 Properties after a connection

Due to the multilaterals, flow will mix at some points of the wells. These points are, in general, the kick off points. At the kick off point, the fluid flowing from the vertical segment below, and from its branch is mixed and the properties will need to be recalculated. Here, we present the equations for the properties at a vertical segment k, with a segment $k+1$ connected below, and a branch k connected to its kick off point.

The new oil rate at standard condition is simply the sum of the two flow rates converging into the connection.

$$q_{ostd}^{v,k} = q_{ostd}^{v,k+1} + q_{ostd}^{b,k}, \tag{26}$$

where the superscripts v and b denote a vertical section and a branched section, respectively.

A material balance revealed that the gas gravity could be approximated through the following averaging.

$$\gamma_g^{v,k} = \frac{GOR^{v,k+1} q_{ostd}^{v,k+1} \gamma_g^{v,k+1} + GOR^{b,k} q_{ostd}^{b,k} \gamma_g^{b,k}}{GOR^{v,k+1} q_{ostd}^{v,k+1} + GOR^{b,k} q_{ostd}^{b,k}}. \quad (27)$$

where *GOR* is the gas oil ratio.

For averaging the API gravity, we first convert it to specific density using the API formula, and them we apply the following averaging:

$$SG_{ostd}^{v,k} = \frac{q_{ostd}^{v,k+1} SG_{ostd}^{v,k+1} + q_{ostd}^{b,k} SG_{ostd}^{b,k}}{q_{ostd}^{v,k+1} + q_{ostd}^{b,k}}, \quad (28)$$

and then

$$\gamma_o^{v,k} = \frac{141.5}{SG_{ostd}^{v,k}} - 131.5. \quad (29)$$

The *GOR* is computed by simply summing all the gas volume that would be produced independently at surface and dividing it by the overall oil volume that would be produce as below:

$$GOR^{v,k} = \frac{q_{gstd}^{v,k+1} + q_{gstd}^{b,k}}{q_{ostd}^{v,k+1} + q_{ostd}^{b,k}}. \quad (30)$$

2.5 Reservoir Material Balance

In this work, the reservoir is approximated using a “tank model”. In this model, the properties are assumed to change uniformly along the whole reservoir. The full material balance equation is used (Economides et al., 1994):

$$F = N\left[E_o + mE_g + E_{f,w}\right], \quad (31)$$

where *N* is the initial oil in place, *m* is the ratio of the initial gas cap volume to the initial volume of the oil zone, E_o is the oil expansivity, E_g is the gas expansivity, and $E_{f,w}$ is the rock and water combined expansivity, and are computed as

$$F = N_p\left(B_o + \left(R_p - R_s\right)B_g\right), \quad (32)$$

$$E_o = \left(B_o - B_{oi}\right) + \left(R_{si} - R_s\right)B_g, \quad (33)$$

$$E_g = B_{oi}\left(\frac{B_g}{B_{gi}} - 1\right), \quad (34)$$

and

$$E_{f,w} = \left(1+m\right)B_{oi}\left(\frac{c_w S_{wc} + c_f}{1 - S_{wc}}\right)\left(P - \mathrm{P}_{ref}\right). \quad (35)$$

where N_p is the cumulative oil production, R_p is the producing gas-oil ratio, B_g is the gas formation volume factor, B_{gi} and B_{oi} are the gas an oil formation volume factors before production, S_{wc} is the water critical saturation, c_f is the rock compressibility and P_{ref} is a reference pressure.

The method used here was developed to allow us to work with several reservoirs at the same time. In our method, instead of calculating a change in time from a given change in pressure as some models in the literature, we set a change in time and calculate the change in pressure for each reservoir. This method is convenient here because it ensures that the time-step is always the same no matter how many reservoirs are being considered. In this method, we start computing the change in the oil and gas recoveries for each reservoir through the following explicit approximation:

$$\Delta N_{p,i} = q_{o,i}\Delta t, \qquad i = 1,\ldots,n_l\,, \tag{36}$$

and

$$\Delta G_{p,i} = q_{g,i}\Delta t, \qquad i = 1,\ldots,n_l\,, \tag{37}$$

where G_p is the cumulative gas production, n_l is the number of laterals/reservoirs considered.

Consider Eq. (31) written for a time $t+\Delta t$ below:

$$F_{i,t+\Delta t} = N\left[E_{oi,t+\Delta t} + mE_{gi,t+\Delta t} + E_{f,wi,t+\Delta t}\right], \qquad i = 1,\ldots,n_l\,. \tag{38}$$

Each term in Eq. (38) can be approximated through a Taylor series truncated in the first term

$$F_{i,t+\Delta t} = F_{i,t} + \frac{dF_{i,t}}{dt}\Delta t, \qquad i = 1,\ldots,n_l\,, \tag{39}$$

$$E_{oi,t+\Delta t} = E_{oi,t} + \frac{dE_{oi,t}}{dt}\Delta t, \qquad i = 1,\ldots,n_l\,, \tag{40}$$

$$E_{gi,t+\Delta t} = E_{gi,t} + \frac{dE_{gi,t}}{dt}\Delta t, \qquad i = 1,\ldots,n_l\,, \tag{41}$$

and

$$E_{f,w,i,t+\Delta t} = E_{f,w,i,t} + \frac{dE_{f,w,i,t}}{dt}\Delta t, \qquad i = 1,\ldots,n_l\,. \tag{42}$$

The first term is then written as

$$\begin{aligned} F_{i,t+\Delta t} &= N_{p,i,t}\left(B_{o,i,t} + \left(R_{p,i,t} - R_{s,i,t}\right)B_{g,i,t}\right) \\ &\quad + \frac{d}{dt}\left[N_{p,i,t}\left(B_{o,i,t} + \left(R_{p,i,t} - R_{s,i,t}\right)B_{g,i,t}\right)\right]\Delta t, \qquad i = 1,\ldots,n_l \end{aligned}\,. \tag{43}$$

Therefore,

Proceedings of the XXXVIII Iberian Latin-American Congress on Computational Methods in Engineering
P.O. Faria, R.H. Lopez, L.F.F. Miguel, W.J.S. Gomes, M. Noronha (Editores), ABMEC, Florianópolis, SC, Brazil, November 5-8, 2017.

$$
\begin{aligned}
F_{i,t+\Delta t} &= N_{p,i,t}\left(B_{o,i,t}+\left(R_{p,i,t}-R_{s,i,t}\right)B_{g,i,t}\right)\\
&+\left(B_{o,i,t}+\left(R_{p,i,t}-R_{s,i,t}\right)B_{g,i,t}\right)\frac{dN_{p,i,t}}{dt}\Delta t\\
&+N_{p,i,t}\left(\frac{dB_{o,i,t}}{dt}\Delta t+\left(\frac{dR_{p,i,t}}{dt}\Delta t-\frac{dR_{s,i,t}}{dt}\Delta t\right)B_{g,i,t}+\left(R_{p,i,t}-R_{s,i,t}\right)\frac{dB_{g,i,t}}{dt}\Delta t\right), \quad i=1,\ldots,n_l
\end{aligned}
\quad , \quad (44)
$$

where

$$
\frac{dN_{p,i,t}}{dt}\Delta t = N_{p,i,t+\Delta t}-N_{p,i,t}=\Delta N_{p,i,t}\,, \quad (45)
$$

and

$$
\frac{dR_{p,i,t}}{dt}\Delta t = R_{p,i,t+\Delta t}-R_{p,i,t}=\Delta R_{p,i,t}\,, \quad (46)
$$

where

$$
\Delta R_{p,i,t}=\frac{G_{p,i,t}+\Delta G_{p,i,t}}{N_{p,i,t}+\Delta N_{p,i,t}}-\frac{G_{p,i,t}}{N_{p,i,t}}\,. \quad (47)
$$

Notice that pressure is a function of time, and all reservoir properties are in fact functions of pressure. This allow us to use the chain rule

$$
\frac{dB_{o,i,t}}{dt}\Delta t=\frac{dB_{o,i,t}}{dP}\frac{dP}{dt}\Delta t=\frac{dB_{o,i,t}}{dP}\Delta P\,, \quad (48)
$$

$$
\frac{dB_{g,i,t}}{dt}\Delta t=\frac{dB_{g,i,t}}{dP}\frac{dP}{dt}\Delta t=\frac{dB_{g,i,t}}{dP}\Delta P\,, \quad (49)
$$

and

$$
\frac{dR_{s,i,t}}{dt}\Delta t=\frac{dR_{s,i,t}}{dP}\frac{dP}{dt}\Delta t=\frac{dR_{s,i,t}}{dP}\Delta P\,. \quad (50)
$$

Therefore,

$$
\begin{aligned}
F_{i,t+\Delta t} &= N_{p,i,t}\left(B_{o,i,t}+\left(R_{p,i,t}-R_{s,i,t}\right)B_{g,i,t}\right)+\left(B_{o,i,t}+\left(R_{p,i,t}-R_{s,i,t}\right)B_{g,i,t}\right)\Delta N_{p,i}\\
&+N_{p,i,t}\left(\frac{dB_{o,i,t}}{dP}\Delta P+\left(\Delta R_{p,i}-\frac{dR_{s,i,t}}{dP}\Delta P\right)B_{g,i,t}+\left(R_{p,i,t}-R_{s,i,t}\right)\frac{dB_{g,i,t}}{dP}\Delta P\right)
\end{aligned}
\quad , \quad (51)
$$

and

$$
\begin{aligned}
F_{i,t+\Delta t} &= N_{p,i,t+\Delta t}\left(B_{o,i,t}+\left(R_{p,i,t}-R_{s,i,t}\right)B_{g,i,t}\right)+N_{p,i,t}B_{g,i,t}\Delta R_{p,i}\\
&+N_{p,i,t}\left(\frac{dB_{o,i,t}}{dP}-\frac{dR_{s,i,t}}{dP}B_{g,i,t}+\left(R_{p,i,t}-R_{s,i,t}\right)\frac{dB_{g,i,t}}{dP}\right)\Delta P
\end{aligned}
\quad . \quad (52)
$$

The right hand side of Eq. (38) is written as

Proceedings of the XXXVIII Iberian Latin-American Congress on Computational Methods in Engineering
P.O. Faria, R.H. Lopez, L.F.F. Miguel, W.J.S. Gomes, M. Noronha (Editores), ABMEC, Florianópolis, SC, Brazil, November 5-8, 2017.

$$N_i\begin{bmatrix}\left(B_{o,i,t+\Delta t}-B_{oi}\right)+\left(R_{si,i}-R_{s,i,t+\Delta t}\right)B_{g,i,t+\Delta t}+m_iB_{oi,i}\left(\frac{B_{g,i,t+\Delta t}}{B_{gi,i}}-1\right)\\+\left(1+m_i\right)B_{oi,i}\left(\frac{c_{w,i}s_{wc,i}+c_{f,i}}{1-s_{wc,i}}\right)\left(P_{i,t+\Delta t}-P_{ref,i}\right)\end{bmatrix}$$

$$=N_i\begin{bmatrix}\left(B_{o,i,t}-B_{oi,i}\right)+\left(R_{si,i}-R_{s,i,t}\right)B_{g,i,t}+m_iB_{oi,i}\left(\frac{B_{g,i,t}}{B_{gi,i}}-1\right)\\+\left(1+m_i\right)B_{oi,i}\left(\frac{c_{w,i}s_{wc,i}+c_{f,i}}{1-s_{wc,i}}\right)\left(P_{i,t}-P_{ref,i}\right)\end{bmatrix}$$

$$+\frac{d}{dt}\left\{N_i\begin{bmatrix}\left(B_{o,i,t}-B_{oi,i}\right)+\left(R_{si,i}-R_{s,i,t}\right)B_{g,i,t}+m_iB_{oi,i}\left(\frac{B_{g,i,t}}{B_{gi,i}}-1\right)\\+\left(1+m_i\right)B_{oi,i}\left(\frac{c_{w,i}s_{wc,i}+c_{f,i}}{1-s_{wc,i}}\right)\left(P_{i,t}-P_{ref,i}\right)\end{bmatrix}\right\}\Delta t \quad , \qquad (53)$$

which after some manipulation reduces to

$$N_i\begin{bmatrix}\left(B_{o,i,t+\Delta t}-B_{oi}\right)+\left(R_{si,i}-R_{s,i,t+\Delta t}\right)B_{g,i,t+\Delta t}+m_iB_{oi,i}\left(\frac{B_{g,i,t+\Delta t}}{B_{gi,i}}-1\right)\\+\left(1+m_i\right)B_{oi,i}\left(\frac{c_{w,i}s_{wc,i}+c_{f,i}}{1-s_{wc,i}}\right)\left(P_{i,t+\Delta t}-P_{ref,i}\right)\end{bmatrix}$$

$$=N_i\begin{bmatrix}\left(B_{o,i,t}-B_{oi,i}\right)+\left(R_{si,i}-R_{s,i,t}\right)B_{g,i,t}+m_iB_{oi,i}\left(\frac{B_{g,i,t}}{B_{gi,i}}-1\right)\\+\left(1+m_i\right)B_{oi,i}\left(\frac{c_{w,i}s_{wc,i}+c_{f,i}}{1-s_{wc,i}}\right)\left(P_{i,t}-P_{ref,i}\right)\end{bmatrix} \quad . \qquad (54)$$

$$+N_i\begin{bmatrix}\frac{dB_{o,i,t}}{dP}-\frac{\partial R_{s,i,t}}{\partial P}B_{g,i,t}-\frac{\partial B_{g,i,t}}{\partial P}R_{s,i,t}\\+m_i\frac{B_{oi,i}}{B_{gi,i}}\frac{dB_{g,i,t}}{dP}+\left(1+m_i\right)B_{oi,i}\left(\frac{c_{w,i}s_{wc,i}+c_{f,i}}{1-s_{wc,i}}\right)\end{bmatrix}\Delta P_i$$

Combining Eqs. (52) and (54) we obtain

$$
\begin{aligned}
&N_{p,i,t+\Delta t}\left(B_{o,i,t}+\left(R_{p,i,t}-R_{s,i,t}\right)B_{g,i,t}\right)+N_{p,i,t}B_{g,i,t}\Delta R_{p,i}\\
&+N_{p,i,t}\left(\frac{dB_{o,i,t}}{dP}-\frac{dR_{s,i,t}}{dP}B_{g,i,t}+\left(R_{p,i,t}-R_{s,i,t}\right)\frac{dB_{g,i,t}}{dP}\right)\Delta P_i=\\
&N_i\begin{bmatrix}\left(B_{o,i,t}-B_{oi,i}\right)+\left(R_{si,i}-R_{s,i,t}\right)B_{g,i,t}+m_iB_{oi,i}\left(\dfrac{B_{g,i,t}}{B_{gi,i}}-1\right)\\ +\left(1+m_i\right)B_{oi,i}\left(\dfrac{c_{w,i}s_{wc,i}+c_{f,i}}{1-s_{wc,i}}\right)\left(P_{i,t}-P_{ref,i}\right)\end{bmatrix}.\\
&+N_i\begin{bmatrix}\dfrac{dB_{o,i,t}}{dP}-\dfrac{\partial R_{s,i,t}}{\partial P}B_{g,i,t}-\dfrac{\partial B_{g,i,t}}{\partial P}R_{s,i,t}\\ +m_i\dfrac{B_{oi,i}}{B_{gi,i}}\dfrac{dB_{g,i,t}}{dP}+\left(1+m_i\right)B_{oi,i}\left(\dfrac{c_{w,i}s_{wc,i}+c_{f,i}}{1-s_{wc,i}}\right)\end{bmatrix}\Delta P_i
\end{aligned}
\tag{55}
$$

Say

$$a_i=N_{p,i,t+\Delta t}\left(B_{o,i,t}+\left(R_{p,i,t}-R_{s,i,t}\right)B_{g,i,t}\right)+N_{p,i,t}B_{g,i,t}\Delta R_{p,i}\,, \tag{56}$$

$$a_{p,i}=N_{p,i,t}\left(\frac{dB_{o,i,t}}{dP}-\frac{dR_{s,i,t}}{dP}B_{g,i,t}+\left(R_{p,i,t}-R_{s,i,t}\right)\frac{dB_{g,i,t}}{dP}\right), \tag{57}$$

$$b_i=N_i\begin{bmatrix}\left(B_{o,i,t}-B_{oi,i}\right)+\left(R_{si,i}-R_{s,i,t}\right)B_{g,i,t}+m_iB_{oi,i}\left(\dfrac{B_{g,i,t}}{B_{gi,i}}-1\right)\\ +\left(1+m_i\right)B_{oi,i}\left(\dfrac{c_{w,i}s_{wc,i}+c_{f,i}}{1-s_{wc,i}}\right)\left(P_{i,t}-P_{ref,i}\right)\end{bmatrix}, \tag{58}$$

and

$$b_{p,i}=N_i\begin{bmatrix}\dfrac{dB_{o,i,t}}{dP}-\dfrac{\partial R_{s,i,t}}{\partial P}B_{g,i,t}-\dfrac{\partial B_{g,i,t}}{\partial P}R_{s,i,t}\\ +m_i\dfrac{B_{oi,i}}{B_{gi,i}}\dfrac{dB_{g,i,t}}{dP}+\left(1+m_i\right)B_{oi,i}\left(\dfrac{c_{w,i}s_{wc,i}+c_{f,i}}{1-s_{wc,i}}\right)\end{bmatrix}. \tag{59}$$

Therefore, the pressure increments for each time-step can be computed as

$$\Delta P_i=\frac{b_i-a_i}{a_{p,i}-b_{p,i}}\,. \tag{60}$$

and

$$P_{i,t+\Delta t}=P_{i,t}+\Delta P_i\,. \tag{61}$$

Notice that this approach provides the pressure increments without no iteration. Readers may be careful by selecting the time-step size. Large time-step may lead to unstable solution,

Proceedings of the XXXVIII Iberian Latin-American Congress on Computational Methods in Engineering
P.O. Faria, R.H. Lopez, L.F.F. Miguel, W.J.S. Gomes, M. Noronha (Editores), ABMEC, Florianópolis, SC, Brazil, November 5-8, 2017.

as a result of the explicit formulation described above. Also, the derivatives of the reservoir fluid properties are required. Next, we present the equations used to calculate the derivatives of the properties with respect to pressure.

The water saturation for each time-step is computed as

$$S_{w,t+\Delta t} = S_{wc}\,\frac{1+c_w\left(P_{i,t+\Delta t}-P_{ref,i}\right)}{1+c_f\left(P_{i,t+\Delta t}-P_{ref,i}\right)}. \tag{62}$$

The oil saturation

$$S_{o,t+\Delta t} = \left(1-S_{w,t+\Delta t}\right)\frac{\left(N_i-N_{p,i,t+\Delta t}\right)B_{o,i,t+\Delta t}}{\left[\left(N_i-N_{p,i,t+\Delta t}\right)\left(B_{o,i,t+\Delta t}-R_{s,i,t+\Delta t}\right)+G_i-G_{p,i,t+\Delta t}\right]}, \tag{63}$$

and the gas saturation

$$S_{g,t+\Delta t} = \left(1-S_{w,t+\Delta t}-S_{g,t+\Delta t}\right). \tag{64}$$

The relative permeabilities are calculated using Corey's model

$$k_{rw} = k_{rw}^0\left(\frac{S_w-\min\left(S_w,S_{wr}\right)}{1-\min\left(S_w,S_{wr}\right)-\min\left(S_o,S_{or}\right)-\min\left(S_g,S_{gr}\right)}\right)^{e_w}, \tag{65}$$

$$k_{ro} = k_{ro}^0\left(\frac{S_o-\min\left(S_o,S_{or}\right)}{1-\min\left(S_w,S_{wr}\right)-\min\left(S_o,S_{or}\right)-\min\left(S_g,S_{gr}\right)}\right)^{e_o}, \tag{66}$$

and

$$k_{rg} = k_{rg}^0\left(\frac{S_g-\min\left(S_g,S_{gr}\right)}{1-\min\left(S_w,S_{wr}\right)-\min\left(S_o,S_{or}\right)-\min\left(S_g,S_{gr}\right)}\right)^{e_g}, \tag{67}$$

where the water saturation is assumed to be always below the residual water saturation, meaning that the water relative permeability will always be assumed to be zero in this work.

The reservoir's bubble-point pressure will be controlled based on the oil and gas in place assuming the following equation (adapted from Vazquez and Beggs, 1980):

$$P_b = \begin{cases} \left(\dfrac{27.64}{10^{\frac{11.172\gamma_o}{T+460}}\gamma_g}\,\dfrac{G-G_p}{N-N_p}\right)^{\frac{1}{1.0937}} & for\ \ \gamma_o \le 30^o\,API \\[2ex] \left(\dfrac{56.06}{10^{\frac{10.393\gamma_o}{T+460}}\gamma_g}\,\dfrac{G-G_p}{N-N_p}\right)^{\frac{1}{1.187}} & for\ \ \gamma_o > 30^o\,API \end{cases}. \tag{68}$$

Equation (68) is important because it shows that, for a saturated reservoir, the bubble point pressure at which a gas cap appears is not the same as the bubble pressure when we start to produce.

The initial oil saturation is computed as

$$S_{o,i} = \left(1 - S_{w,i}\right) \frac{B_{oi}}{\left[B_{oi} + \left(R_{sbi} - R_{si} \right) B_{gi} \right]}, \tag{69}$$

where R_{sbi} is the gas oil ratio evaluated at the initial bubble point pressure.

The initial oil in place is computed as

$$N = S_{o,i} \frac{Ah\phi}{B_{oi}}, \tag{70}$$

where A is the drainage area, and $S_{o,i}$ is the initial oil saturation, and the initial gas in place

$$G = R_{sbi} N. \tag{71}$$

The ratio between the gas cap volume and the oil volume is computed as

$$m = \frac{\left(R_{sbi} - R_{si} \right) B_{gi}}{B_{oi}}. \tag{72}$$

3 ALGORITHMS AND NUMERICAL METHODS

The simulator developed in this work has a general pressure traverse algorithm that allows it to solve the fluid flow in wells with any number of laterals. The algorithm initializes the pressure at the kickoff points using a linear interpolation with the well head pressure and the highest reservoir pressure. Curved sections are paired with vertical sections, where a vertical section is considered between kickoff points or between the well head and the first kickoff point. The iterative approach starts by solving pressure distribution at the deepest curved section to match the guessed KOP pressure. Subsequently, the rate obtained is used to calculate the pressures at the vertical section and matching the guess for the higher KOP. This procedure will change the value of the lower KOP that will need to have the pressure distribution of the associated branch solved again. For a branch *k* associated with a KOP *k*, the algorithm for solving the pressure distribution is given in Figure 2a. The algorithm for calculating the pressure in a vertical section *k*, between KOP's *k* and *k-1* is presented in Figure 2b. The algorithm for converging the KOP pressures along with the whole profile is a recursive subroutine and is described in Figure 3. Notice that the recursive algorithm will fully solve the problem if *k1* is set to *1*. Figure 4 presents the algorithm for the whole simulator, considering the reservoir and well coupling.

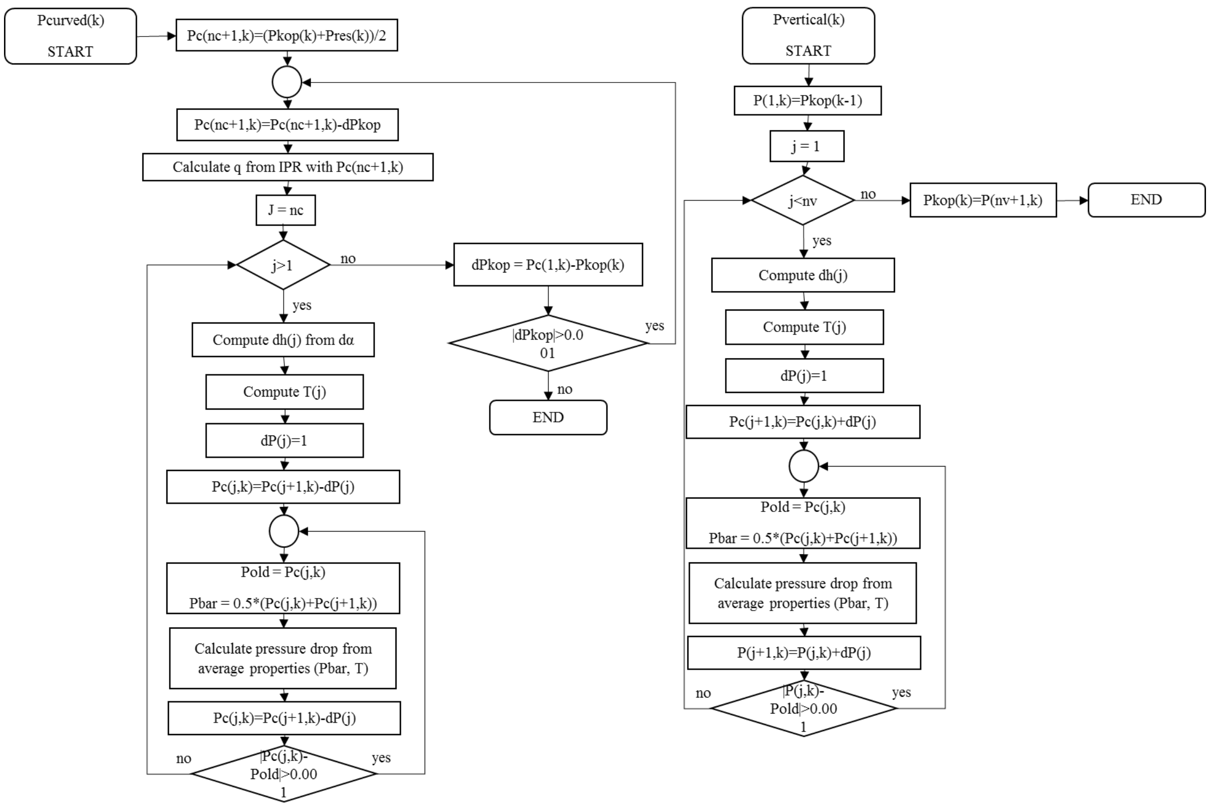

(a) (b)

Figure 2. Algorithm for computing pressure distribution. a) in a branch; b) in a vertical section.

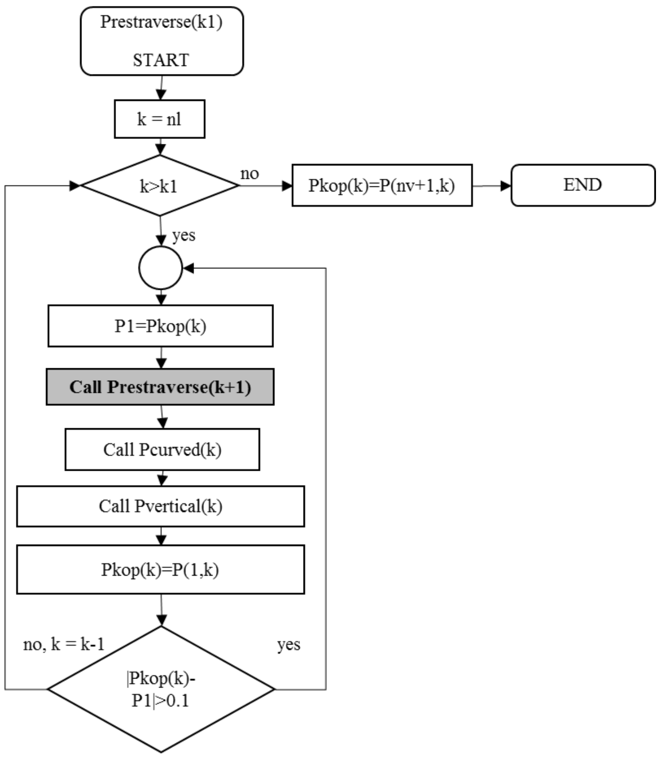

Figure 3. Algorithm for the pressure traverse algorithm.

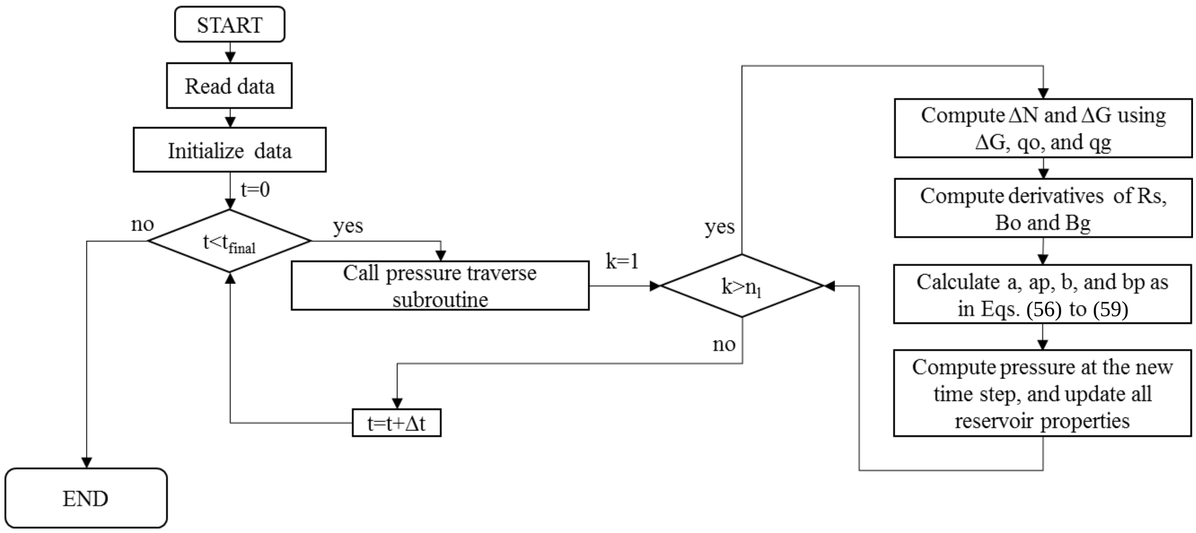

Figure 4. Software workflow.

4 RESULTS

A case study considering three different oil bearing formations at different depths is considered. The formations do not communicate, and a lateral is drilled through each of the formations. We will refer each formation as reservoir 1, 2, and 3. The common data is presented in Table 1. The data for the fluids and reservoirs are presented in Table 2.

Table 1. Common data.

Property	Value
Well head pressure	0.483 MPa
Tubing string diameter	0.1016 m
Tubing roughness	0.0508 mm
Total time	2500 days
Time-step	5 days
Well head temperature	341.83 K

The pressure distribution from the beginning of the simulation is compared to that obtained at 2500 days in Figures 5a and 5b. It can be observed that not only the pressure values at the reservoirs are smaller, due to the reservoir depletion, but there is also a change in the inclination of the curves, which results from the changes in fluid composition, and the change in the velocities along the well (which produces less friction losses).

The amount of pressure drop caused by the hydrostatic pressure is also presented in Figure 6, where it can be observed that it has much smaller contribution closer to the well head. This is expected because the gas is released as the fluids move upward. Since gas is less dense, the gravitational effects become smaller. On the other hand, it should be noticed from Figure 5, that the pressure drop becomes bigger closer to the surface, which is a result, mainly, of the increase in velocity experienced by the gas phase, producing large friction.

The flow patterns are presented in Figure 7. Because we do not consider friction losses in the curved sections and no special flow pattern, we present the flow patterns for the vertical region only. It can be observed that mist flow is achieved at the beginning of the simulation close to the well head, but most of the well operates at the slug flow. At the end of the simulation, no mist flow is obtained, but bubble flow is observed at the bottom of the well.

Table 2. Data for each reservoir and lateral.

Property	**Reservoir/Lateral 1**	**Reservoir/Lateral 2**	**Reservoir/Lateral 3**
Bottom hole temperature	361.11 K	377.38 K	380.49 K
Kick off point	914.4 m	1584.96 m	1737.36 m
Curvature radius	91.44 m	91.44 m	91.44 m
Reservoir thickness	12.192 m	35.052 m	16.1544 m
Lateral length	609.6 m	121.92 m	152.4 m
Lateral radius	0.0381 m	0.0381 m	0.0381 m
Drainage area	4.047×10^6 m^2	2.023×10^6 m^2	1.214×10^6 m^2
Formation Permeability	1.480×10^{-15} m^2	1.283×10^{-14} m^2	8.093×10^{-15} m^2
Skin factor	0	0	0
Reservoir pressure	20 MPa	27.92 MPa	35.51 MPa
Bubble point pressure	31.03 MPa	30 MPa	41.53 MPa
Oil API gravity	38 API	42 API	46 API
Gas specific gravity	0.8	0.71	0.75

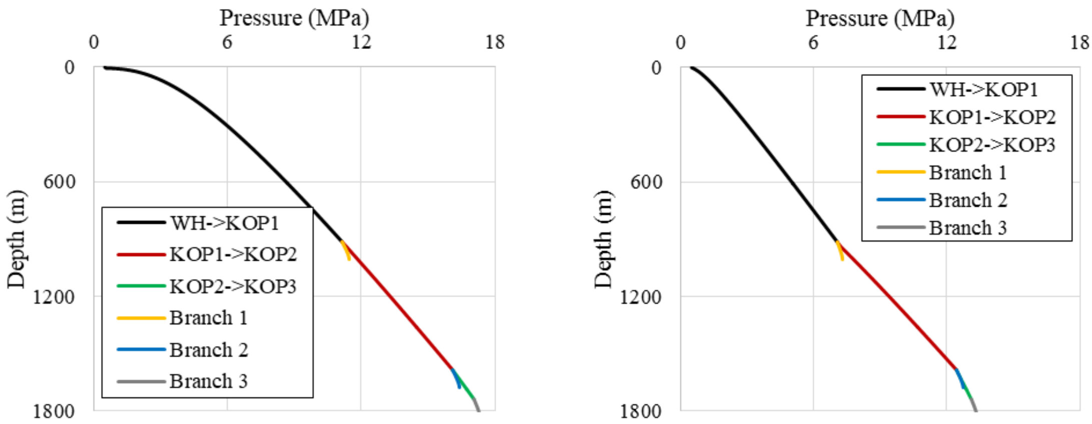

(a) (b)

Figure 5. Pressure profile. a) at 0 days; b) at 2500 days.

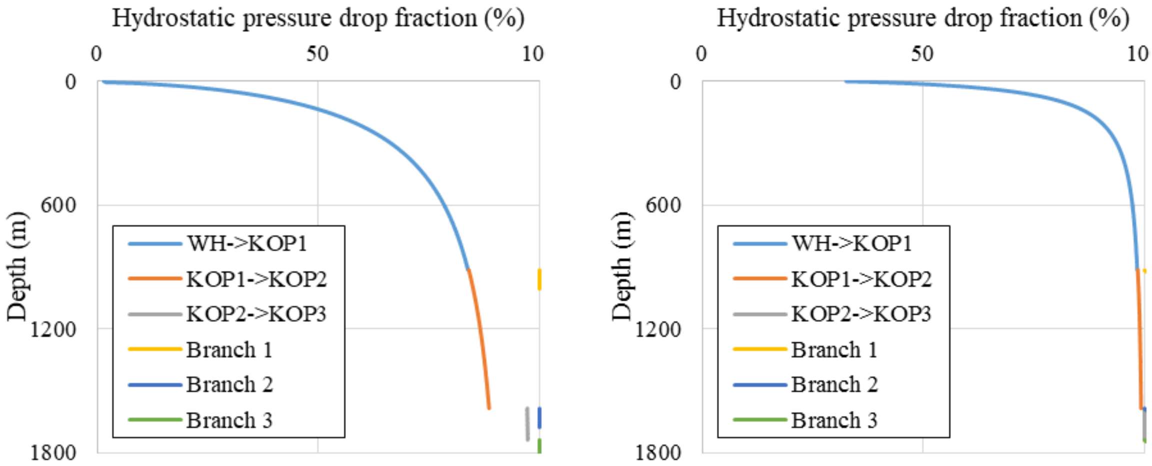

(a) (b)

Figure 6. Hydrostatic pressure drop fraction. a) at 0 days; b) at 2500 days.

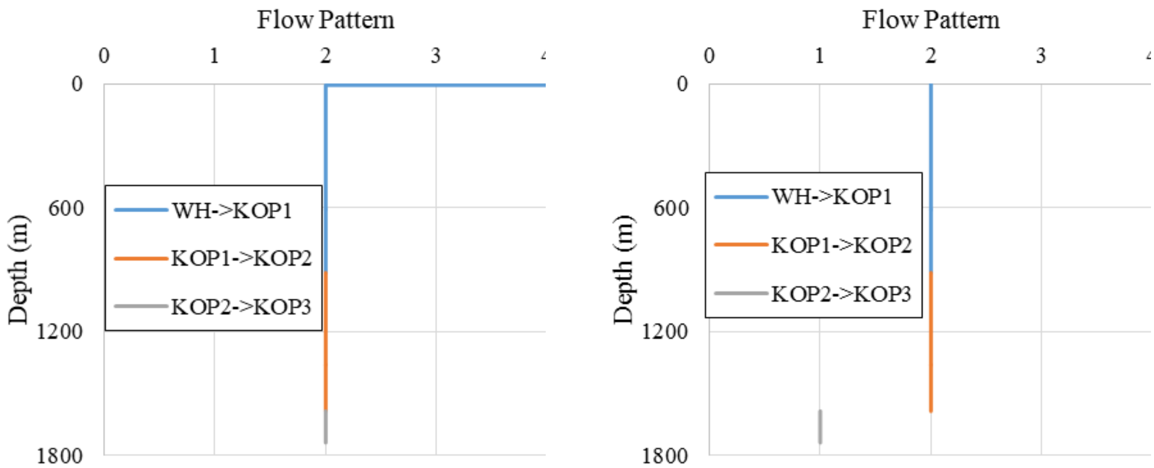

(a) (b)

Figure 7. Flow regimes along the well (0-single phase; 1-Bubble flow; 2-Slug flow; 3-Transition flow; 4-Mist flow). a) at 0 days; b) 2500 days.

The coupling between the wellbore and the reservoirs is also useful to provide some production forecast. The oil rates from each reservoir and the total oil rate are presented in Figure 8a. Similarly, the gas rate is presented in Figure 8b. It can be noticed that the reservoirs produce at very different rates, which happens for two reasons: the first is the reservoir productivity for its given pressure, while the second is the well deliverability problem. Since three different reservoirs are producing at the same time, it may occur that different reservoirs reduce the productivity of others. In Figure 8c, it can be observed that Reservoir 3 has produced about 70% of its oil, while Reservoir 1 produced only 5%. The overall oil recovery was about 50% of the total oil reserves. To increase the oil production from Reservoir 1, it would be necessary to decrease the well head pressure or use a lift technique to provide more energy to Reservoir 1. The pressure of the reservoirs can also be monitored as observed in Figure 8d. It should be noticed that several parameters should be optimized in the design of such wells, like the well-head pressure, tubing diameter, lateral lengths, among others. The tool presented in this work may be used for such task in future projects.

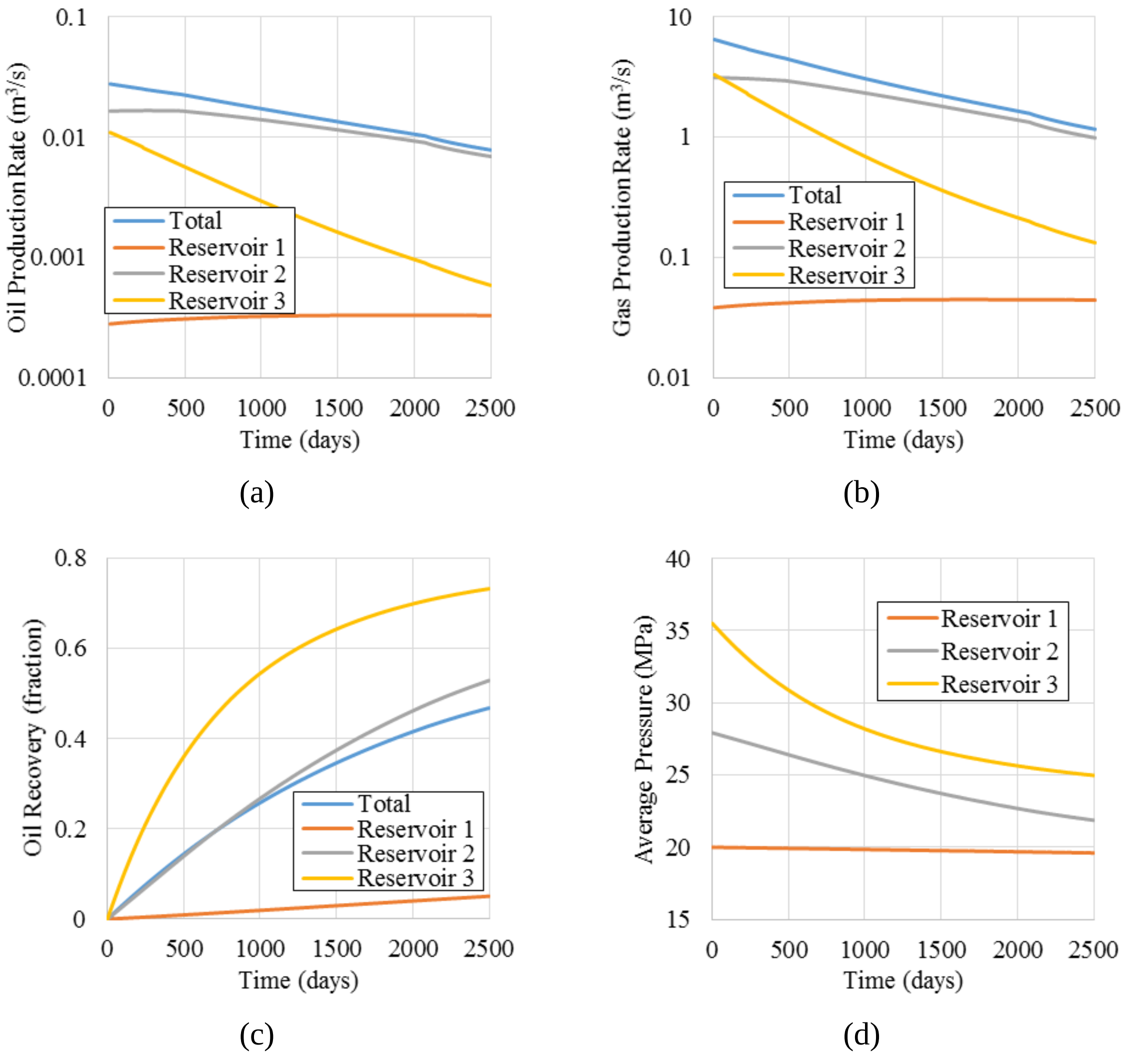

Figure 8. Forecasting. a) Oil production rate; b) Gas production rate; c) Oil Recovery; d) Reservoir average pressure.

5 CONCLUSIONS

A new tool for coupling subsurface and surface parameters in oil and gas wells has been developed. The new developed tool considers several multiphase flow patterns along the well and the possibility of several connections to the main string. A new algorithm for computing the pressure distribution for an arbitrary number of laterals was presented.

The tool was coupled to the simplistic “tank model” oil reservoirs to provide the production forecast of such reservoirs. A procedure for obtaining production rates and reservoir pressures for a given time-steps was also proposed. The coupling of such tool to more complex reservoir simulators follows the same procedure and may be considered in the future.

Finally, the tool was successful in simulating the pressure profile along production tubing and showed that friction losses cannot be ignored when compared to hydrostatic pressure drop.

ACKNOWLEDGEMENTS

The first author would like to acknowledge CNPq (The National Council for Scientific and Technological Development of Brazil) for its financial support. The authors also would like to thank Dr. Quoc Nguyen for his important guidance and discussions in this project. We would also like to thanks Petrobras for financing support of this study.

REFERENCES

Bendakhlia, H., & Aziz, K., 1989. Inflow Performance Relationships for Solution-Gas Drive Horizontal Wells, *SPE Annual Technical Conference and Exhibition*.

Bird, R. B., Stewart, W. E., & Lightfoot, E. N., 2007. *Transport Phenomena*. Revised 2nd Ed., John Willey & Sons.

Brill, J. P. & Beggs, H. D., 1973. A Study of Two-Phase Flow in Inclined Pipes. *Journal of Petroleum Technology*, vol. 25, n. 5, pp. 607-617.

Brown, K. E., 1977. *The Technology of Artificial Lift Methods, vol. 1*. Pennwell Books.

Chen, N. H., 1979. An Explicit Equation for Friction Factor in Pipe. *Industrial and Engineering Chemistry Fundamentals*, vol. 18, pp. 296-297.

Colebrook, C. F., & White, C. M., 1937. Experiments with Fluids Friction in Roughened Pipes, In: *Proceedings of the Royal Society of London: Series A, Mathematics and Physical Sciences*, vol. 161, pp. 367-381.

Economides, M. J., Hill, A. D., & Economides, C. E., 1994. *Petroleum Production Systems*, Prentice Hall, New Jersey.

Hagedorn, A. R. & Brown, K. E., 1965. Experimental Study of Pressure Gradients Occurring During Continuous Two-Phase Flow in Small-Diameter Vertical Conduits. *Journal of Petroleum Technology*, vol. 17, n. 4, pp. 475-484.

Nguyen, Q. P., *Lecture Notes: Wellbore Flow Performance: Gas-Liquid Flow*, The university of Texas at Austin. 2016.

Orkiszewski, J., 1967. Predicting Two-Phase Pressure Drops in Vertical Pipe, *Journal of Petroleum Technology*. vol. 19, pp. 829-838.

Shirdel, M. & Sepehrnoori, K., 2012. Development of a Transient Mechanistic Two-Phase Flow Model for Wellbores. *SPE Journal*, vol. 17, n. 3, pp. 942-955.

Taitel, Y. & Dukler, A. E., 1976. A model for predicting flow regime transitions in horizontal and near horizontal gas-liquid flow. *AIChE Journal*, vol. 22, pp. 47–55.

Taitel, Y., Bornea, D. & Dukler, A. E., 1980. Modelling flow pattern transitions for steady upward gas-liquid flow in vertical tubes. *AIChE Journal*, vol. 26, pp. 345–354.

Vazquez, M. & Beggs, H. D., 1980. Correlation for Fluid Physical Property Prediction. *Journal of Petroleum Technology*, vol. 32, n. 6, pp. 968-970.